Quasar Black Hole Masses and Accretion Rates Across Cosmic Time

Michael Brotherton¹, Jaya Maithil¹, Adam Myers¹, Ohad Shemmer², Brandon Matthews², Cooper Dix², Pu Du³, & Jian-Min Wang³

¹Dept. of Physics & Astronomy, University of Wyoming, Laramie, WY 82071, USA email: mbrother@uwyo.edu

Abstract. Quasar black hole masses are most commonly estimated using broad emission lines in single epoch spectra based on scaling relationships determined from reverberation mapping of small samples of low-redshift objects. Several effects have been identified requiring modifications to these scaling relationships, resulting in significant reductions of the black hole mass determinations at high redshift. Correcting these systematic biases is critical to understanding the relationships among black hole and host galaxy properties. We are completing a program using the Gemini North telescope, called the Gemini North Infrared Spectrograph (GNIRS) Distant Quasar Survey (DQS), that has produced rest-frame optical spectra of about 200 high-redshift quasars (z = 1.5-3.5). The GNIRS-DQS will produce new and improved ultraviolet-based black hole mass and accretion rate prescriptions, as well as new redshift prescriptions for velocity zero points of high-z quasars, necessary to measure feedback.

Keywords. quasars: general, quasars: emission lines

1. Introduction

There exist a number of outstanding questions regarding supermassive black holes, where they come from, how they grow, and how they interact with their host galaxies. Two fundamental properties of populations of supermassive black holes that can be better determined with careful observations are their masses and accretion rates across cosmic time.

2. Quasar Black Hole Mass Estimation

While there are a number of methods of determining the mass of a supermassive black hole, reverberation mapping (RM) is the primary technique used to make direct mass measurements for luminous active galactic nuclei (AGNs) such as Seyfert galaxies and quasars (e.g., Peterson et al. 1993). Spectroscopic monitoring can reveal the time delay between the variable continuum and the corresponding response from an extended broadline region (BLR), which is governed by its spatial extent due to the finite speed of light. In combination with BLR velocities, obtained from the Doppler-broadened emission-line profiles, the time delays can be used to determine a virial mass for the central supermassive black hole:

$$M_{\rm BH} = f_{\rm BLR} \frac{R_{\rm BLR} \Delta V^2}{G},\tag{2.1}$$

²Department of Physics, University of North Texas, Denton, TX 76203, USA

 $^{^3{\}rm Key}$ Laboratory for Particle Astrophysics, Institute of High Energy Physics, Chinese Academy of Sciences, 19B Yuquan Road, Beijing 100049, People's Republic of China

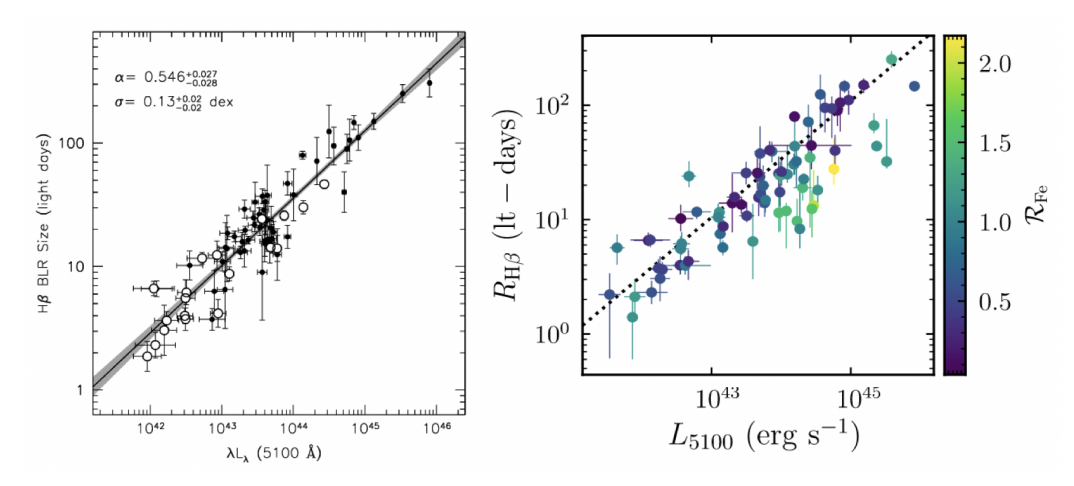


Figure 1. The radius-luminosity relationship for reverberation-mapped AGNs. Left. Bentz et al. (2013). Right. Du & Wang (2019), which includes a color scheme indicating the strength of the optical Fe II blend relative to the broad H β line. AGNs with strong Fe II have systematically shorter time lags.

where $R_{\rm BLR} = c\tau_{\rm BLR}$ is the emissivity-weighted radius of the BLR, c is the speed of light, G is the gravitational constant, and (ΔV) is measured from the FWHM or line dispersion (e.g., Peterson et al. 2004). The factor $f_{\rm BLR}$ is an empirically calibrated geometric correction factor of order unity (e.g., Woo et al. 2015). The value of $f_{\rm BLR}$ in individual objects likely differs due to effects such as inclination (e.g., Pancoast et al. 2014).

The recognition that there was a correlation between AGN luminosity and the H β time lag (e.g., Kaspi et al. 2000) led to the development of mass estimation based on single-epoch spectra (e.g., Vestergaard 2000; Vestergaard & Peterson 2006). Increasing reverberation mapping efforts led to a relatively tight relationship of: $\tau_{\rm H}_{\beta} \propto \lambda L_{\lambda_{5100}}^{0.54}$ (Bentz et al. 2013; Fig. 1, left).

Reverberation-mapped samples up to that time were biased, however, to have strong narrow [O III] $\lambda\lambda4959,5007$ emission lines, which help with flux calibration due to their very slow variability. Reverberation mapping of AGNs with weak [O III] lines (which also have strong broad optical Fe II emission, see, e.g. Boroson & Green 1992), turn out to deviate from the scaling relationship of Bentz et al. (2013) and have much shorter than expected H β time lags by factors of 3-8 times in the most extreme objects (Fig. 1, right). They also have large accretion rates (Shen & Ho 2014; Du et al. 2018). This deviation in the time lag can be predicted by the strength of the ratio of optical Fe II to H β emission, R_{FeII} (Du & Wang 2019), leading to a revised scaling relationship unbiased by accretion rate: log ($\tau_{\rm H}\beta$ /lt-days) = 1.65 + 0.45 log ($\lambda L_{\lambda_{5100}}$ /10⁴⁴ ergs/s) -0.35 R_{FeII}.

Two parameters are used in describing accretion rates that depend on both the luminosity and the black hole mass. The Eddington fraction is $L_{\rm Bol}/L_{\rm Edd},$ which requires a bolometric correction, and scales simply as $L/M_{\rm BH}.$ Another normalized accretion rate can be estimated by the formula

$$\dot{M} = 20.1 \left(\frac{\ell_{44}}{\cos i}\right)^{3/2} m_7^{-2},$$
 (2.2)

where $m_7 = M_{\rm BH}/10^7 M_{\odot}$, and i is inclination angle of the accretion disk (with $\cos i = 0.75$ as an average value for AGNs). Based on the standard α -disk model (Shakura

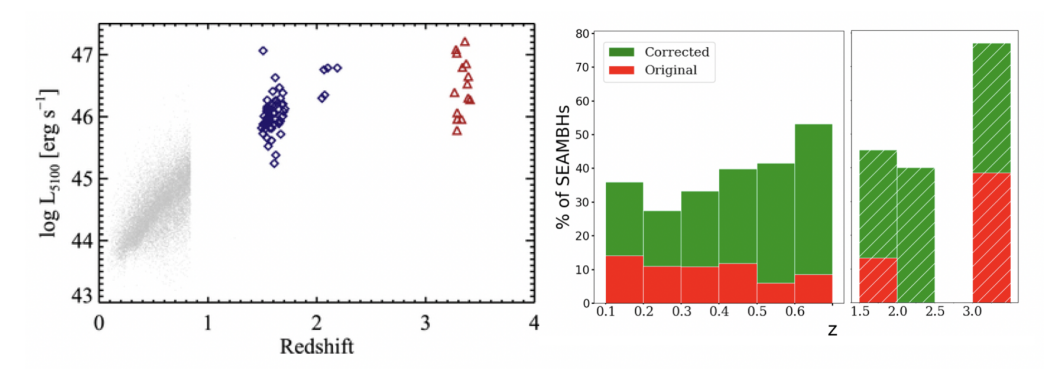


Figure 2. Left. The luminosity-redshift plane for our quasar samples. The gray points are from the SDSS sample using measurements from Shen et al. (2011). The points with z>1.5 are from Shen (2016). Right. Histograms of the percentage of objects in each redshift bin with $\dot{M}>3$ (Super-Eddington Accreting Massive Black Holes, or SEAMBHs) for the old scaling relation of Bentz et al. (2013) (red) and the new scaling relation of Du & Wang (2019) (green). Using the new scaling relation indicates a much higher fraction of highly accreting quasars that is likely higher at high-z.

& Sunyaev 1973), quasars with values of $\dot{M}>3$ will be considered Super Eddington Accreting Massive Black Holes (SEAMBHs) for the present discussion, and we note that this parameter scales as L/M $_{\rm BH}^2$ (see Du & Wang 2019 and references therein for more discussion and details).

3. New Black Hole Masses and Accretion Rates over Cosmic Time

Using the revised scaling relationship of Du & Wang (2019), we have calculated new black hole masses and accretion rates (M) for two samples of quasars for which luminosities, $H\beta$ line widths, and R_{FeII} have been measured. At lower redshifts we use the Shen et al. (2011) catalog for the Sloan Digital Sky Survey (SDSS) Data Release 7 Quasar Sample, only keeping objects with measurements having signal-to-noise ratios greater than 10 (totaling 1487 objects). At higher redshifts (z = 1.5 - 3.5) we use a compilation of 74 objects by Shen (2016) based on near-infrared spectra of the redshifted H β spectral region. Figure 2 shows the luminosity-redshift space and histograms of the fraction having super-Eddington accretion rates (M > 3) using masses based on the Bentz et al. (2013) (red) and the Du & Wang (2019) (green) scaling relations. The masses for the latter are rather smaller on average and the accretion rates higher. We see that with previous calibrations, only a small fraction of quasars are SEAMBHs, but with the new calibration there is quite a large fraction that increases with redshift. This reflects the fact that high-z quasars have systematically different rest-frame optical properties with larger $R_{\rm FeII}$ than those at low-z, and that the luminous quasars at "cosmic noon" have larger accretion rates.

The SDSS provides many tens of thousands of observed-frame optical spectra for quasars with z>1.5, but only a tiny minority of these have rest-frame optical spectra. Without an ultraviolet proxy for the accretion rate, which $R_{\rm FeII}$ acts as at optical wavelengths, the masses and accretion rates are systematically wrong by sometimes very significant factors.

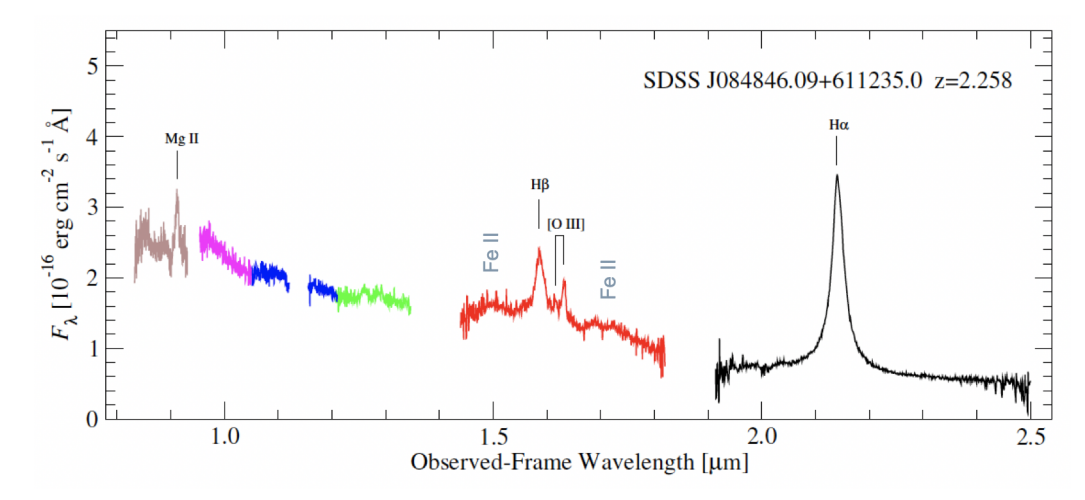


Figure 3. An example spectrum of a GNIRS DQS quasar selected from the SDSS. Prominent emission lines of interest are marked. The six GNIRS bands are distinguished using different colors. Regions of low signal-to-noise ratio where atmospheric absorption are large have been excluded.

4. The GNIRS Distant Quasar Survey (GNIRS GDQS)

In 2017, we launched a program to increase the quantity of high-quality near-infrared spectra of representative quasars between redshifts of 1.5 and 3.5 (Mathews et al. 2018, 2019, 2020). We selected bright, luminous objects from the SDSS that already possessed good quality rest-frame ultraviolet spectra, including radio-quiet, radio-loud, and broad absorption line (BAL) quasars. Over the last three years we have used the GNIRS instrument on Gemini-North to obtain approximately 200 high-quality near-infrared spectra of the rest-frame optical spectrum ensuring that the H β region, including the [O III] and Fe II lines, were generally centered in an observing band. Figure 3 shows an example GDQ spectrum.

A primary goal of this project is to assemble a data set that will enable us to calculate the most precise and accurate black hole masses, accretion rates, and redshifts of the luminous quasars at cosmic noon using the best methodologies, which rely on rest-frame optical spectral measurements. These in turn will be compared in a consistent manner with those of quasars at lower redshifts for a relatively unbiased look at quasars across cosmic time. Above and beyond simply establishing the black holes masses and accretion rates of the luminous quasars at cosmic noon, we will also be able to construct ultraviolet estimations for black hole mass and accretion rate that correct the systematic biases that exist in current formulations. We anticipate that a combination of measurements using the prominent Mg II and C IV ultraviolet emission lines can do the job. This work can then be used for the tens of thousands of high-z quasars with SDSS spectra to establish the demographics of actively accreting supermassive black holes.

The narrow [O III] $\lambda5007$ line is the preferred redshift reference for quasars at optical wavelengths (Boroson 2005). In the near-ultraviolet, the peak of the Mg II broad line provides a reasonably good measure of systematic redshift (Tytler & Fan 1992), but it is not always available in the spectra of distant quasars. We have also been pioneering a simple prescription using the prominent ultraviolet C IV line to measure accurate and precise redshifts despite the line's history as unsuitable due to its consistent blueshift (Mason, Brotherton, & Myers 2017; Dix et al. 2020). The new GNIRS DQS data set will allow us to significantly refine our formula. These improved redshifts will better estab-

lish zero points for the absorption and emission features characteristic of outflows that demonstrate an extreme signature of quasar feedback. Better redshift estimates can also improve a range of studies at high redshift, for example, quasar clustering measurements.

5. Conclusions

We conclude that using the most up-to-date scaling relationships reveals that the black hole masses of the luminous quasars at cosmic noon have been significantly overestimated, and the accretion rates underestimated. With the GNIRS GDQS we will robustly quantify these statements and develop new and improved ultraviolet-based prescriptions for black hole mass and accretion rate, as well as redshift.

6. Acknowledgments

JMW acknowledges the support from the National Science Foundation of China (NSFC-11833008 and -11991054), from the National Key R&D Program of China (2016YFA0400701). PD acknowledges the support from NSFC-11873048, -11991051 and the Strategic Priority Research Program of the Chinese Academy of Sciences (XDB23010400). This work is supported by National Science Foundation grants AST-1815281 and AST-1815645.

References

Bentz, M. C., Denney, K. D., Grier, C. J., et al. 2013, ApJ, 767, 149

Boroson, T. 2005, AJ, 130, 381

Boroson, T. A., & Green, R. F. 1992, ApJS, 80, 109

Du, P., & Wang, J.-M. 2019, ApJ, 886, 42

Du, P., Zhang, Z.-X., Wang, K., et al. 2018, ApJ, 856, 6

Dix, C., Shemmer, O., Brotherton, M. S., et al. 2020, ApJ, 893, 14

Kaspi, S., Smith, P. S., Netzer, H., et al. 2000, ApJ, 533, 631

Matthews, B., Shemmer, O., Brotherton, M., et al. 2020, American Astronomical Society Meeting Abstracts, 381.06

Matthews, B., Shemmer, O., Brotherton, M. S., et al. 2019, American Astronomical Society Meeting Abstracts #233, 243.38

Matthews, B., Shemmer, O., Brotherton, M. S., et al. 2018, American Astronomical Society Meeting Abstracts #232, 318.09

Mason, M., Brotherton, M. S., & Myers, A. 2017, MNRAS, 469, 4675

Pancoast, A., Brewer, B. J., Treu, T., et al. 2014, MNRAS, 445, 3073

Peterson, B. M. 1993, PASP, 105, 247

Peterson, B. M., Ferrarese, L., Gilbert, K. M., et al. 2004, ApJ, 613, 682

Shakura, N. I., & Sunyaev, R. A. 1973, $A \mathcal{B} A$ 500, 33

Shen, Y. 2016, ApJ, 817, 55

Shen, Y., & Ho, L. C. 2014, Nature, 513, 210

Shen, Y., Richards, G. T., Strauss, M. A., et al. 2011, ApJS, 194, 45

Tytler, D., & Fan, X.-M. 1992, ApJS, 79, 1

Vestergaard, M. 2002, ApJ, 571, 733

Vestergaard, M., & Peterson, B. M. 2006, ApJ, 641, 689

Woo, J.-H., Yoon, Y., Park, S., et al. 2015, ApJ, 801, 38